PCCP

PAPER

View Article Online
View Journal | View Issue

Cite this: *Phys. Chem. Chem. Phys.*, 2018, **20**, 1497

A comprehensive study of catalytic, morphological and electronic properties of ligand-protected gold nanoclusters using XPS, STM, XAFS, and TPD techniques†

Qiyuan Wu, ‡[a] Jiajie Cen,‡[a] Yue Zhao, [b] Xiao Tong,[c] Yuanyuan Li,[a] Anatoly I. Frenkel,[ad] Shen Zhao*[e] and Alexander Orlov*[a]

Received 17th September 2017,
Accepted 8th December 2017

DOI: 10.1039/c7cp06376h

rsc.li/pccp

Ultra-small gold nanoclusters were synthesized *via* a ligand exchange method and deposited onto different TiO_2 supports to study their properties. STM imaging revealed that the as-synthesized gold nanoclusters had 2-D morphology consisting of monolayers of gold atoms. Subsequent XPS, XAFS, and CO oxidation TPD results indicated that heat treatments of gold clusters at different temperatures significantly altered their electronic and catalytic properties due to ligand deprotection and cluster agglomeration.

Introduction

Metal nanoclusters (NCs) are very promising catalysts for a number of different applications.[1–6] For many years, bulk Au was considered to be inert and therefore an ineffective material for catalytic applications. However, this notion has substantially evolved following the discovery of the Au size-effect, where Au particles of few nm in size were shown to exhibit catalytic activity.[7–9] Reducing the Au size to even smaller dimensions appears to be the next logical step in exploring its chemistry. It was previously reported that the catalytic activity of supported Au NCs depends on the number of Au atoms contained in the NC.[10–12] Therefore, a more granular knowledge of the size effect of Au NCs is needed to tune their unique properties to facilitate chemical reactions.[1,13–23] In addition to the size, the geometry of these NCs may prove to be another important parameter to tune their properties, given that the coordination of Au atoms and the NC electronic structure are shape dependent, especially for sub-nm dimensions[24,25] It is also important to note that the shape of supported NCs is often an overlooked parameter in the published literature, where the size of NCs is used as a primary factor to explain their catalytic activity. Unfortunately, despite impressive advances in microscopy techniques, a reliable determination of the Au NC shape as a size-averaged parameter still remains a challenge.[22,26,27]

In addition to describing challenges in NC characterization, it is also important to outline different approaches to their synthesis.[1,11,28–32] Among several synthetic methods, the size-selected cluster (SSC) approach is the one providing a very good control over the cluster size, while producing extremely clean NCs under ultra-high vacuum (UHV) conditions. Importantly, this approach has an advantage over other methods of NC synthesis, given that the clusters produced *via* the SSC method can be characterized *in situ* during the synthesis.[33,34] The size selected approach also has disadvantages as compared to more traditional chemical synthesis methods. For example, the SSC method is regarded as being much less scalable and more difficult to use for NC deposition onto complex three-dimensional substrates as compared to the alternative methods. In addition to consideration of the cluster size, it is also important to highlight the effect of surface modification on the catalytic activity. The synthetic methods achieving a good control over the cluster size often utilize ligands or surfactants to control the size of clusters during the chemical synthesis of NCs. Such a control over the cluster size also has notable disadvantages as ligands and surfactants can block active sites on supported NC surfaces, thereby requiring additional treatment to activate them for catalytic applications. Therefore, developing scalable methods of the synthesis of NCs, while understanding and optimizing both the cluster size and surface coverage/deprotection, is an important topic of research.

[a] *Department of Material Science and Chemical Engineering, Stony Brook University, Stony Brook, NY 11794, USA. E-mail: alexander.orlov@stonybrook.edu*
[b] *Department of Chemistry, Stony Brook University, Stony Brook, NY 11794, USA*
[c] *Center for Functional Nanomaterials, Brookhaven National Laboratory, Upton, NY 11973, USA*
[d] *Division of Chemistry, Brookhaven National Laboratory, Upton, NY 11973, USA*
[e] *Energy & Environment, Southern Research, Durham, NC 27712, USA. E-mail: szhao@southernresearch.org*

† Electronic supplementary information (ESI) available: Supporting figures and table. See DOI: 10.1039/c7cp06376h

‡ Equal contribution.

In this work, Au NCs were synthesized *via* a ligand exchange method using diphosphine ligands and deposited onto both TiO_2 single crystals and powder supports to understand their behavior in model and practical catalytic systems. The supported Au NCs were subjected to heat treatments at different temperatures based on a published protocol for the activation of supported ligand-protected Au clusters.[16,35–37] The Au NCs supported on single crystals were imaged using a scanning tunneling microscope (STM). Additionally, X-ray photoelectron spectroscopy (XPS), temperature-programmed desorption (TPD) for CO oxidation, and *in situ* X-ray absorption fine structure (XAFS) spectroscopy including both X-ray absorption near edge structure (XANES) and extended X-ray absorption fine structure (EXAFS) spectroscopies were utilized to examine the evolution of Au NCs as a function of temperature. The novelty of this work is in the utilization of distinct ligand-protected clusters coupled with comprehensive elucidation of their properties using a combination of microscopy and spectroscopy techniques.

Experimental

Synthesis and deposition of Au NCs

Au NCs were synthesized following procedures developed by our group, which were based on modification of the previously published ligand exchange approach.[2,3,31] Briefly, $Au(PPh_3)Cl$ was dissolved in $CHCl_3$ to reach a final concentration of 10^{-3} mol L^{-1}. About 10^{-3} mol L^{-1} $P(PPh)_2(CH_2)_4P(PPh)_2$ was then added to the mixture to achieve the target cluster size. Finally, 5×10^{-3} mol L^{-1} of the reducing agent ($NaBH_4$) was added under continuous stirring for 24 hours at room temperature to produce the Au NC suspension. The as-synthesized Au NC suspension was characterized using UV-Visible spectroscopy (Thermo Evolution 300) and matrix-assisted laser desorption/ionization-time of flight mass spectroscopy (MALDI-TOF MS, Bruker AutoFlex II system). To deposit Au NCs onto the TiO_2 single crystal (rutile, 110), the Au NC suspension was transferred to a manifold and degassed. The manifold was then connected to the load lock chamber of the UHV system. Deposition was controlled through an electromagnetic pulse valve (Parker). To deposit 2.5 wt% Au NCs onto TiO_2(rutile) powders, about 200 mg TiO_2 was added to 20 mL of dichloromethane, followed by addition of the Au NC suspension. The mixture was then stirred overnight to evaporate the solvent.

UHV experiment

STM imaging was carried out using a RHK STM 5000 microscope operating in a constant current mode. The TiO_2 single crystal was first treated according to an Ar^+ sputtering–annealing cleaning procedure to reach atomically flat and clean surfaces, as confirmed by STM images. Au NCs were then deposited onto the TiO_2 single crystal located in the load lock chamber *via* an electromagnetic pulse valve (Parker). After the deposition, the Au NC modified TiO_2 single crystal was again imaged using the STM. After heating the sample at different temperatures (300 K, 373 K, 423 K, and 523 K) for 30 min, the surfaces were characterized using XPS and TPD. XPS measurements were carried out using a hemispherical electron energy analyzer with X-rays generated by a non-monochromatic Al Kα (1486.6 eV) source. Analysis of the XPS spectra was performed using the XPSPEAK version 4.1 software. The Ti $2p_{3/2}$ signal at 458.5 eV was used to calibrate the energy scale to which all the measured binding energies were adjusted, with the Shirley background applied to all spectra. ^{13}C labeled ^{13}CO was used in the TPD experiment in order to exclude the interference of CO_2 present in the chamber, which also includes CO_2 originated from the oxidation of surface contaminants. The TPD experiment was conducted as following: firstly, the sample was cooled to 90 K using liquid N_2, then O_2 was dosed at 10^{-5} Torr and 90 K for 15 minutes following by the sample exposure to ^{13}CO at 4×10^{-5} Torr for 15 minutes. Large exposure of gases was performed here in order to ensure the saturation coverage. Meanwhile, it has been shown that, for the Au catalyst for the CO oxidation reaction, the order of exposure of reactant gases does not change the activity.[32] The sample was then heated to different target temperatures at a ramping rate of 30 K min^{-1}. The upper temperature for the TPR experiment was set to be equal to the heat treatment temperature. The rational for such temperature selection was based on consideration of NC stability during the CO oxidation experiment. During the TPD experiment, the desorbed species were detected using a quadrupole mass spectrometer (MS). Measurements of catalytically produced $^{13}CO_2$ were based on the "m/z = 45" signal.

In situ XANES measurement

In situ XAS measurements were performed at Beamline ×18B (NSLS, Brookhaven National Laboratory). The Au L_3 edge spectra of 2.5 wt% Au/TiO_2 catalysts were collected in the fluorescence mode. The sample powders were pressed into pellets and mounted into a custom-designed and -built catalyst cell. Subsequently, He gas was introduced to the cell using a mass flow controller. Spectra were collected upon different heat treatments.

Results and discussion

Fig. 1a shows the STM image of a clean TiO_2(110)-(1 × 1) surface. The image indicates the presence of terraces with a width of a few hundred Å and steps with a height of ~3 Å, which is consistent with the expected step height for a rutile(110)-(1 × 1) surface described in the literature.[34,38] Fig. 1b shows the STM image of a clean TiO_2 surface at a higher magnification. The alternating bright and dark lines correspond to 5-fold coordinated Ti atom (5c-Ti) rows and bridging oxygen rows, respectively. The separation of ~6.5 Å between neighboring Ti atom rows is also consistent with the published literature.[34,39]

Following the imaging of the TiO_2(110)-(1 × 1) surface, it was modified with Au NCs, which were delivered *via* an electromagnetic pulse valve. Fig. 2a–c show the STM images of an Au NC modified TiO_2 surface at different magnifications.

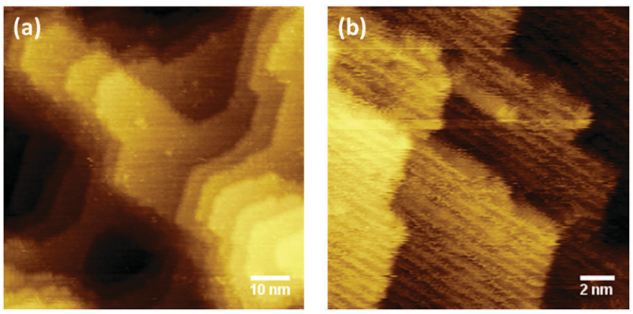

Fig. 1 STM images of a clean TiO_2(110)-(1 × 1) surface at low magnification (a) and high magnification (b). The alternating bright and dark lines in (b) corresponded to 5-fold coordinated Ti atom (5c-Ti) rows and bridging oxygen rows, respectively.

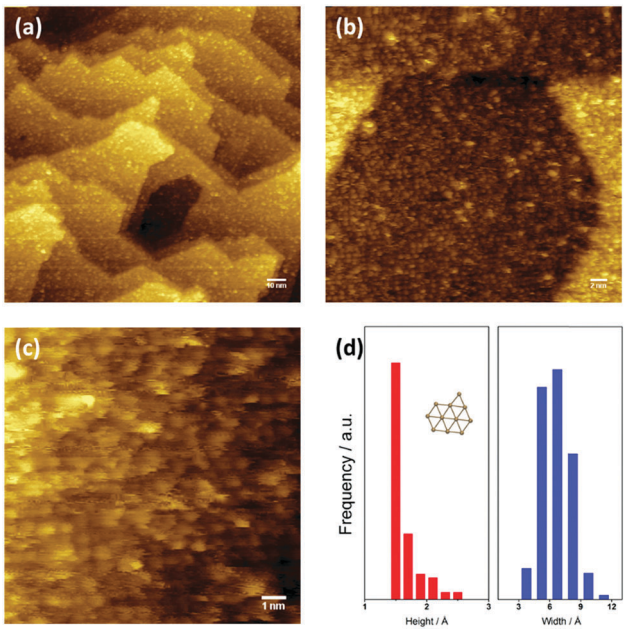

Fig. 2 STM images of Au NCs supported on a TiO_2 surface and size distribution of Au NCs. (a–c): STM images of Au NCs at different magnifications; (d) height and width distribution of Au NCs; the inset of (d) shows one of the calculated optimized geometries of Au NCs from our previous work.[3]

At low magnification (Fig. 2a), the Au NCs appeared as uniform particles with the width of ~2 nm. However, higher magnification images (Fig. 2b and c, and Fig. S1 in ESI†) reveal that these particles were formed from smaller Au NCs. It is worth noting that the results described above suggest that this method of deposition is promising for producing high coverage layers of small size of NCs, which is often a challenging task for traditional deposition approaches. The height and width distributions of Au NCs based on Fig. 2b are presented in Fig. 2d. The average height and width of the supported Au NCs were about 1.6 Å and 6.5 Å, respectively. A typical line scan of two Au NCs is shown in Fig. S2, ESI.† Given these dimensions, one may conclude that the Au NCs consisted of one atomic layer of ~10 Au atoms. Such a conclusion agrees well with our previous work showing that the Au NCs synthesized *via* this ligand exchange approach contain 8–11 Au atoms.[2] The uniformity of the synthesized Au NCs was also confirmed using UV-Visible spectroscopy and MALDI-TOF mass spectroscopy as shown in Fig. S3, ESI.† Furthermore, our previous published theoretical calculations (insert of Fig. 2d) have shown that one of the optimized geometries of Au NCs consisting of 11 Au atoms has only one layer of Au atoms.[3] In order to benchmark our results against the already available literature, we analyzed the published studies on Au NCs containing ~10 Au atoms. Although these studies proposed several stable geometries of Au NCs containing ~10 Au atoms, one has to be careful in directly comparing them to our work, given that characterization approaches and synthetic methods described in the literature were quite different from ours.[13–15,19–22,30,40,41] For example, in one such study, Al Qahtani *et al.* utilized electron microscopy and computational approaches to study the structure of Au NCs consisting of 9 Au atoms.[22] Although the geometry proposed in Al Qahtani's study was consistent with the model proposed here, it is also important to note that our STM data are more representative of the shape of NCs as compared to that deduced from TEM results.[22] Following the STM imaging, the samples were characterized using XPS. Fig. 3a shows the Au 4f XPS spectrum of the as-deposited Au NCs. This spectrum could be fitted with only one doublet, indicating a fairly uniform chemical state of Au NCs. The binding energy of the Au $4f_{7/2}$ electron was 86.1 eV, which is higher than both the value of 84.0 eV characteristic of bulk Au and the value of 85.6 eV of the precursor gold complex.[42] Literature analysis indicated that the shift can be explained by different factors, including the high oxidation state of clusters and their small size,[18,43] and cluster–substrate and cluster–ligand interactions, leading to a cluster charge.[16,17,22] In our case, the small size effect should be the least significant factor in explaining the 1.6 eV shift from the binding energy of metallic gold, given that the literature described binding energy of the Au $4f_{7/2}$ electron of ligand-free Au clusters consisting of only 2 Au atoms was only 84.8 eV.[18] In addition to the importance of ligand–cluster interactions to explain the observed shifts, cluster–support interactions should also be considered. For example, published data show 2-D Au NCs consisting of 11 Au atoms would have strong interaction with the TiO_2 substrate, resulting in a shift of the binding energy of the Au $4f_{7/2}$ electron towards higher binding energy.[16] Finally, the contribution of the high oxidation state of Au should be considered in explaining our data as discussed later in the text.

Following the XPS study of the as-deposited Au NCs, the samples were then subjected to different heat treatments to study the evolution of Au NCs. Fig. 2b–d show the Au 4f XPS spectra of Au NCs exposed to heating cycles at 3 discrete temperatures of 373 K, 423 K, and 523 K. The rationale for choosing these temperatures and a holding time of 30 min is explained in the Experimental Method section in the ESI.† It can be clearly seen that Au NCs undergo significant evolution upon heat treatment. More specifically, heating the samples at 373 K for 30 min resulted in the appearance of a new chemical state of Au as indicated by green lines in Fig. 3b. In order to

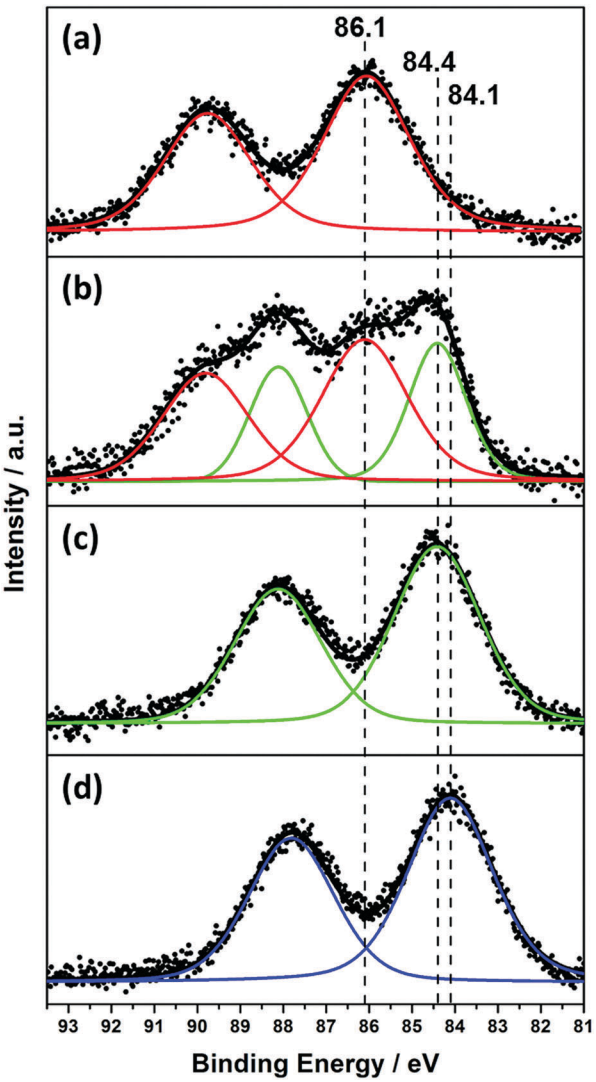

Fig. 3 XPS spectra of Au NCs upon different heating treatments. Black dots are experimental data and colored lines represent fitted lines. (a) As-deposited Au NCs; (b) upon heating at 373 K; (c) upon heating at 423 K; and (d) upon heating at 523 K. The binding energies of the Au $4f_{7/2}$ electron of different species are indicated by the dash lines.

account for these states the Au 4f XPS spectrum was fitted with two doublets. The binding energies for the Au $4f_{7/2}$ electron were determined to be 86.1 eV and 84.4 eV, indicating the formation of a lower binding energy chemical state of Au in addition to a higher binding energy component of the as-deposited Au NCs. The lower binding energy species might have originated from the partial removal of ligands and/or reduction of the as-deposited Au NCs. Further heating of the sample at 423 K for 30 min resulted in a complete disappearance of the 86.1 eV doublet as shown in Fig. 3c. Such disappearance indicates a complete removal of ligands at this temperature, which is also consistent with the published literature.[37] Further heating at 523 K for 30 min resulted in the appearance of a doublet at an even lower electron binding energy of 84.1 eV as indicated by the blue line in Fig. 3d. Given that this binding energy is very similar to that of bulk Au, it suggests the complete reduction of Au species and formation of larger Au particles with properties approaching those of bulk gold. The changes in C and P species were also examined. Fig. S4 in the ESI† shows the C 1s and P 2p XPS spectra of the samples upon heat treatment at different temperatures. No significant changes in C 1s and P 2p spectra as compared to those in Au 4f spectra were observed, indicating that diphosphine ligands remained on the surface after removal from the Au cluster. This conclusion also agrees with the published study where temperatures higher than 523 K were needed to vaporize the diphosphine ligands.[37] STM imaging of samples subjected to heat treatment was also attempted as a part of our characterization efforts. The STM images of the sample heated at 373 K, 423 K, and 523 K are shown in Fig. S5 and S6 in the ESI.† Although the image contrast was not sufficient to conduct reliable statistical analysis of size distribution, Au NCs with the above-mentioned size and geometry still can be seen in the sample heated at 423 K (Fig. S5, ESI†). Furthermore, the presence of large particles with a diameter of ~8.6 nm (Fig. S6b and S6d, ESI†) in the sample heated at 523 K confirmed the formation of larger Au particles with properties approaching those of bulk gold.

The reduction and growth of Au NCs upon heating were then confirmed using *in situ* XAFS. Fig. 4 shows the Au L_3 edge XAFS spectra of the as-deposited Au NCs supported on TiO_2 and that of the heat-treated sample, plotted along with the spectrum of a standard bulk Au foil. The absorption edge intensity in the XANES spectra near the main edge maximum (also known as the white line) is proportional to the empty 5d electron density. In other words, the higher the Au oxidation state, the higher the white line intensity. It can be clearly seen that the heat treatment reduced the Au species as the white line intensity decreased toward that of the Au foil (Fig. 4a). Careful analysis of the spectra revealed that the white line intensity of the heated sample was only slightly higher than that of the standard bulk Au foil, indicating that the chemical state of Au species heated up to 523 K was very close to that of the bulk Au foil. This observation was also consistent with the XPS data (Fig. 3d), where the binding energy (84.1 eV) of the Au $4f_{7/2}$ electron was very close to that of bulk Au (84 eV). In the EXAFS region, it can be clearly seen that the local environment of Au atoms in the as-deposited Au NCs is very different from that in the bulk Au

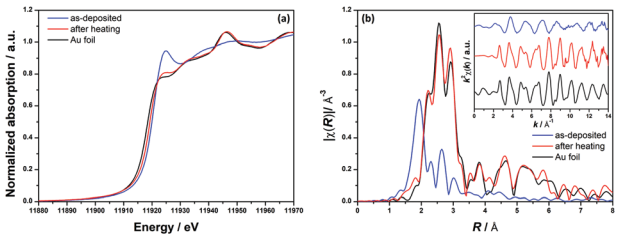

Fig. 4 XAFS spectra of Au NCs before and after heating treatment. (a) XANES spectra of as-deposited and heat-treated Au NCs along with the spectrum of a standard bulk Au foil. (b) Fourier transform magnitude of $k2$ weighted EXAFS data of as-deposited and heat treated Au NCs along with those of the standard bulk Au foil in R space. Inset of (b) shows the EXAFS data in k space.

foil (Fig. 4b). Theoretical fitting results indicated that the average Au–Au coordination number (CN) for the as-deposited Au NCs was 5.4, which is expected for small clusters consisting of ~10 atoms.[44] After heating treatment at 523 K, the local environment of Au atoms in the sample became similar to that in the bulk Au foil (Fig. 4b). Theoretical fitting results also indicate that the average Au–Au CN increased to 10.6 after heating treatment. Such an increase in Au–Au CN suggests the formation of large Au particles, which is consistent with our XPS results. For details of theoretical fitting results of EXAFS data, see Fig. S7 and Table S1 in the ESI.† The overall conclusion from the XAFS analysis, derived from both XANES and EXAFS data, is that the results confirmed the reduction and growth of Au NCs upon heating in line with the XPS and STM results.

In order to evaluate the catalytic activity of heat treated Au NCs, CO oxidation TPD experiments were conducted for samples treated at several different temperatures. The upper temperatures for the corresponding TPD experiments were set as the same as the heat treatment temperatures. Fig. 5 displays the TPD results for CO_2 ($^{13}CO_2$, m/z = 45) originating from CO oxidation on the as-deposited and heat-treated samples. The as-deposited Au NCs did not show CO oxidation activity within the temperature range of 110–300 K. This result was consistent with reports showing the absence of CO oxidation activity up to the temperature of 473 K[45,46] on ligand-protected Au clusters deposited on TiO_2. In contrast to the as-deposited NCs, the samples heated at 373 K for 30 min exhibited CO oxidation activity (Fig. 5b). The broad feature in the temperature range of 130–373 K in Fig. 5b indicates the presence of more than one active site for CO_2 formation and/or reaction pathways as described below. Importantly, the activity of NCs for CO oxidation coincides with the onset of ligand removal, as deduced from XPS results discussed earlier. Further heating at 423 K resulted in several well-defined TPD features (Fig. 5c). These features include two distinct peaks at 200 K and 330 K indicating two different active sites for CO_2 formation and/or reaction pathways. Fig. 5d shows the TPD results for the sample treated at 523 K. The low temperature CO_2 desorption peak shown in Fig. 5c disappeared from the TPD spectrum shown in Fig. 5d, with the appearance of a high temperature CO_2 desorption peak starting at 430 K. In order to explain these results, it is important to correlate these data to the one in the published literature. More specifically, the published literature describes several CO oxidation reaction pathways over TiO_2 supported Au catalysts,[47–51] with a particular emphasis being placed on different origins of active oxygen species. For example, recently Widmann *et al.* suggested that the active oxygen species in low temperature CO oxidation are originated from the absorbed molecular oxygen while those at high temperature originated from lattice oxygen in the support oxide.[52] In both cases, the Au/TiO_2 interface plays an important role. As described in the literature, at low temperature (typically below 150 K), molecular oxygen is adsorbed and activated at the perimeter of the Au/TiO_2 interface. Subsequently, CO adsorbed on either Au or TiO_2 can react with activated oxygen to form CO_2.[49,50] In contrast to the low temperature scenario of dissociated oxygen, at high temperature (typically above 353 K), the lattice oxygen atoms located at the perimeter of the Au/TiO_2 interface can react with the CO adsorbed on Au.[53] As a result of this reaction, oxygen vacancies are generated following the desorption of CO_2 and replenished through interaction with oxygen gas.[47,48,53] It is important to highlight several other differences in reaction pathways at low and high temperatures. While CO_2 formation from CO is considered to be the only reaction pathway at low temperature,[49] the formation of other species, such as carbonates and bicarbonates, has been reported to take place at high temperature.[53,54] Carbonate-like species have been proposed as important CO oxidation intermediates, which then can form CO_2 at higher temperature.[53–55] Given the pathways described above, our results indeed indicate different pathways for CO oxidation at different temperatures. The low temperature CO_2 desorption peak starting at 200 K (Fig. 5c) corresponds to CO_2 formation and desorption resulting from the activated molecular oxygen pathway. In contrast, the high temperature CO_2 desorption peak starting at 330 K corresponds to the formation and desorption of CO_2 resulting from the activated lattice oxygen pathway involving either a direct formation of CO_2 and/or an indirect formation *via* decomposition of carbonate-like species. Meanwhile, the disappearance of the low temperature CO_2 desorption peak during the heating up of the sample to 523 K (Fig. 5d) indicates that the ability of Au/TiO_2 to catalyze CO_2 oxidation through the activated molecular oxygen pathway was inhibited due to the high temperature sample treatment. Furthermore, the shift of the high temperature CO_2 desorption peak (Fig. 5d) from 330 K to 430 K indicates the possible formation of various carbonate-like species, which was confirmed using XPS (Fig. S8, ESI†), that decompose and form CO_2 at temperature higher than that encountered during the direct CO oxidation through the activated lattice oxygen pathway. In addition to the role of oxygen to explain various pathways of CO_2 formation, it is also important to highlight the importance of

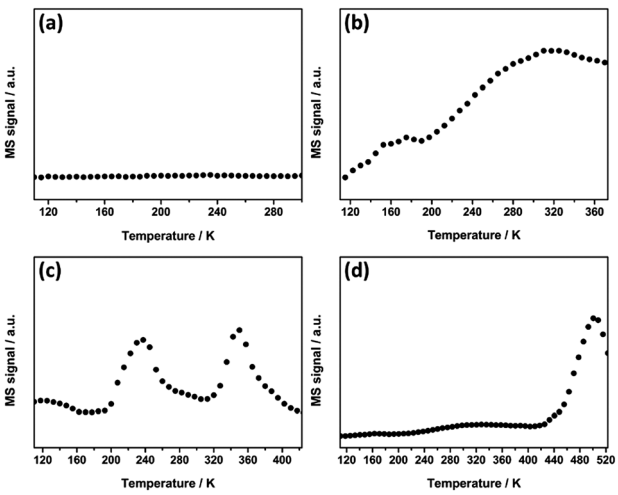

Fig. 5 TPD results of CO oxidation over Au NCs upon different heating treatments. The "m/z = 45" signals representing the production of $^{13}CO_2$ are shown here. (a) As-deposited Au NCs; (b) upon heating at 373 K; (c) upon heating at 423 K; and (d) upon heating at 523 K.

ligand removal for Au NC activation. As shown in Fig. 5a, the as-deposited Au NCs did not exhibit CO oxidation activity, indicating that the ligands probably inhibit the interfacial chemistry of Au/TiO_2 for both low and high temperature oxygen activation pathways, such as molecular oxygen and lattice oxygen atom mechanisms, respectively. The ligands might also prevent CO adsorption and activation.[56–58] The importance of Au NP deprotection to oxidize CO has been examined in a recent study by Wu *et al.*, which indicated that Au NCs containing 22 Au atoms protected by similar diphosphine ligands had mild CO oxidation activity, although the authors also implied that not all the atoms in the NCs were coordinated with ligands and that such uncoordinated Au atoms are essential for catalyzing CO oxidation.[37] In our case, considering that NCs contained around 10 Au atoms, almost every Au atom was coordinated to ligands and thereby exhibited no catalytic activity for CO oxidation. Furthermore, considering the diphosphine ligands possibly stayed on the surface after heat treatments (Fig. S4 (ESI†) and discussion above), the observed activity of Au NCs for CO oxidation indicated that the deprotection of Au NCs was probably more critical than other factors for catalytic application of Au NCs. Given all the above mentioned observations, it is plausible to suggest that removal of ligands is a necessary step to activate Au NCs for CO oxidation.

Conclusions

In conclusion, we successfully synthesized Au NCs through a ligand exchange approach. Detailed characterizations were carried out to study the morphology and electronic properties of these Au NCs. The impact of heat treatment on Au NCs was examined using XPS, *in situ* XAFS, and CO oxidation TPD techniques. We have shown that removal of ligands *via* heat treatment at intermediate temperatures is a critical step to activate very small Au NCs to induce their catalytic activity. However, high temperatures can result in coarsening of Au NCs to form bulk-like large particles, which exhibit lower catalytic activity for CO oxidation as compared to that for smaller particles.

Conflicts of interest

There are no conflicts to declare.

Acknowledgements

We acknowledge funding support from the National Science Foundation (#1254600). We acknowledge the support from the U.S. Department of Energy Grant No. DE-FG02-03ER15476 and Synchrotron Catalysis Consortium (U.S. Department of Energy, Office of Basic Energy Sciences, Grant No. DE-SC0012335). This research used resources of the Center for Functional Nanomaterials, which is a U.S. DOE Office of Science Facility, at Brookhaven National Laboratory under Contract No. DE-SC0012704. We thank Dr Mintcho Tikhov from Cambridge University for helpful discussion.

Notes and references

1 Y. Lu and W. Chen, *Chem. Soc. Rev.*, 2012, **41**, 3594–3623.
2 S. Zhao, G. Ramakrishnan, D. Su, R. Rieger, A. Koller and A. Orlov, *Appl. Catal., B*, 2011, **104**, 239–244.
3 P. Shen, S. Zhao, D. Su, Y. Li and A. Orlov, *Appl. Catal., B*, 2012, **126**, 153–160.
4 Q. Wu, S. Xiong, P. Shen, S. Zhao, Y. Li, D. Su and A. Orlov, *Catal. Sci. Technol.*, 2015, **5**, 2059–2064.
5 Y. Lei, F. Mehmood, S. Lee, J. Greeley, B. Lee, S. Seifert, R. E. Winans, J. W. Elam, R. J. Meyer and P. C. Redfern, *Science*, 2010, **328**, 224–228.
6 R. Siburian, T. Kondo and J. Nakamura, *J. Phys. Chem. C*, 2013, **117**, 3635–3645.
7 G. C. Bond, P. A. Sermon, G. Webb, D. A. Buchanan and P. B. Wells, *J. Chem. Soc., Chem. Commun.*, 1973, 444–445, DOI: 10.1039/C3973000444B.
8 M. Haruta, T. Kobayashi, H. Sano and N. Yamada, *Chem. Lett.*, 1987, 405–408.
9 M. Okumura, S. Nakamura, S. Tsubota, T. Nakamura, M. Azuma and M. Haruta, *Catal. Lett.*, 1998, **51**, 53–58.
10 U. Landman, B. Yoon, C. Zhang, U. Heiz and M. Arenz, *Top. Catal.*, 2007, **44**, 145–158.
11 S. Lee, C. Fan, T. Wu and S. L. Anderson, *J. Am. Chem. Soc.*, 2004, **126**, 5682–5683.
12 X. Tang, J. Schneider, A. Dollinger, Y. Luo, A. S. Worz, K. Judai, S. Abbet, Y. D. Kim, G. F. Gantefor, D. H. Fairbrother, U. Heiz, K. H. Bowen and S. Proch, *Phys. Chem. Chem. Phys.*, 2014, **16**, 6735–6742.
13 F. Wen, U. Englert, B. Gutrath and U. Simon, *Eur. J. Inorg. Chem.*, 2008, 106–111.
14 Y. Shichibu, K. Suzuki and K. Konishi, *Nanoscale*, 2012, **4**, 4125–4129.
15 J. F. Alvino, T. Bennett, D. Anderson, B. Donoeva, D. Ovoshchnikov, R. H. Adnan, D. Appadoo, V. Golovko, G. Andersson and G. F. Metha, *RSC Adv.*, 2013, **3**, 22140–22149.
16 D. P. Anderson, J. F. Alvino, A. Gentleman, H. A. Qahtani, L. Thomsen, M. I. J. Polson, G. F. Metha, V. B. Golovko and G. G. Andersson, *Phys. Chem. Chem. Phys.*, 2013, **15**, 3917–3929.
17 D. P. Anderson, R. H. Adnan, J. F. Alvino, O. Shipper, B. Donoeva, J.-Y. Ruzicka, H. Al Qahtani, H. H. Harris, B. Cowie, J. B. Aitken, V. B. Golovko, G. F. Metha and G. G. Andersson, *Phys. Chem. Chem. Phys.*, 2013, **15**, 14806–14813.
18 S. Peters, S. Peredkov, M. Neeb, W. Eberhardt and M. Al-Hada, *Surf. Sci.*, 2013, **608**, 129–134.
19 J. Chen, Q.-F. Zhang, T. A. Bonaccorso, P. G. Williard and L.-S. Wang, *J. Am. Chem. Soc.*, 2014, **136**, 92–95.
20 F. Dufour, B. Fresch, O. Durupthy, C. Chaneac and F. Remacle, *J. Phys. Chem. C*, 2014, **118**, 4362–4376.

21 L. Yang, H. Cheng, Y. Jiang, T. Huang, J. Bao, Z. Sun, Z. Jiang, J. Ma, F. Sun, Q. Liu, T. Yao, H. Deng, S. Wang, M. Zhu and S. Wei, *Nanoscale*, 2015, **7**, 14452–14459.
22 H. S. Al Qahtani, K. Kimoto, T. Bennett, J. F. Alvino, G. G. Andersson, G. F. Metha, V. B. Golovko, T. Sasaki and T. Nakayama, *J. Chem. Phys.*, 2016, **144**, 114703.
23 H. S. Al Qahtani, G. F. Metha, R. B. Walsh, V. B. Golovko, G. G. Andersson and T. Nakayama, *J. Phys. Chem. C*, 2017, **121**, 10781–10789.
24 B. C. Gates, *Chem. Rev.*, 1995, **95**, 511–522.
25 H. Li, L. Li and Y. Li, *Nanotechnol. Rev.*, 2013, **2**, 515–528.
26 P. D. Jadzinsky, G. Calero, C. J. Ackerson, D. A. Bushnell and R. D. Kornberg, *Science*, 2007, **318**, 430–433.
27 Z. Y. Li, N. P. Young, M. Di Vece, S. Palomba, R. E. Palmer, A. L. Bleloch, B. C. Curley, R. L. Johnston, J. Jiang and J. Yuan, *Nature*, 2008, **451**, 46–48.
28 S. Mostafa, F. Behafarid, J. R. Croy, L. K. Ono, L. Li, J. C. Yang, A. I. Frenkel and B. R. Cuenya, *J. Am. Chem. Soc.*, 2010, **132**, 15714–15719.
29 Q. Wu, C. J. Ridge, S. Zhao, D. Zakharov, J. Cen, X. Tong, E. Connors, D. Su, E. A. Stach, C. M. Lindsay and A. Orlov, *J. Phys. Chem. Lett.*, 2016, **7**, 2910–2914.
30 H. Yao and M. Iwatsu, *Langmuir*, 2016, **32**, 3284–3293.
31 M. F. Bertino, Z.-M. Sun, R. Zhang and L.-S. Wang, *J. Phys. Chem. B*, 2006, **110**, 21416–21418.
32 B. Yoon, H. Häkkinen, U. Landman, A. S. Wörz, J.-M. Antonietti, S. Abbet, K. Judai and U. Heiz, *Science*, 2005, **307**, 403–407.
33 X. Tong, L. Benz, P. Kemper, H. Metiu, M. T. Bowers and S. K. Buratto, *J. Am. Chem. Soc.*, 2005, **127**, 13516–13518.
34 L. Benz, X. Tong, P. Kemper, H. Metiu, M. T. Bowers and S. K. Buratto, *J. Phys. Chem. B*, 2006, **110**, 663–666.
35 M. Turner, V. B. Golovko, O. P. H. Vaughan, P. Abdulkin, A. Berenguer-Murcia, M. S. Tikhov, B. F. G. Johnson and R. M. Lambert, *Nature*, 2008, **454**, 981–983.
36 G. G. Andersson, V. B. Golovko, J. F. Alvino, T. Bennett, O. Wrede, S. M. Mejia, H. S. A. Qahtani, R. Adnan, N. Gunby, D. P. Anderson and G. F. Metha, *J. Chem. Phys.*, 2014, **141**, 014702.
37 Z. Wu, G. Hu, D.-e. Jiang, D. R. Mullins, Q.-F. Zhang, L. F. Allard, L.-S. Wang and S. H. Overbury, *Nano Lett.*, 2016, **16**, 6560–6567.
38 H. Onishi and Y. Iwasawa, *Surf. Sci.*, 1994, **313**, L783–L789.
39 U. Diebold, J. F. Anderson, K.-O. Ng and D. Vanderbilt, *Phys. Rev. Lett.*, 1996, **77**, 1322–1325.
40 J. M. Pettibone, W. A. Osborn, K. Rykaczewski, A. A. Talin, J. E. Bonevich, J. W. Hudgens and M. D. Allendorf, *Nanoscale*, 2013, **5**, 6558–6566.
41 C. C. Chusuei, X. Lai, K. A. Davis, E. K. Bowers, J. P. Fackler and D. W. Goodman, *Langmuir*, 2001, **17**, 4113–4117.
42 Y. M. Shul'ga, A. V. Bulatov, R. A. T. Gould, W. V. Konze and L. H. Pignolet, *Inorg. Chem.*, 1992, **31**, 4704–4706.
43 P. M. T. M. Van Attekum, J. W. A. Van der Velden and J. M. Trooster, *Inorg. Chem.*, 1980, **19**, 701–704.
44 A. I. Frenkel, L. D. Menard, P. Northrup, J. A. Rodriguez, F. Zypman, D. Glasner, S. P. Gao, H. Xu, J. C. Yang and R. G. Nuzzo, *AIP Conf. Proc.*, 2007, **882**, 749–751.
45 X. Nie, H. Qian, Q. Ge, H. Xu and R. Jin, *ACS Nano*, 2012, **6**, 6014–6022.
46 G. Li and R. Jin, *Acc. Chem. Res.*, 2013, **46**, 1749–1758.
47 D. Widmann and R. J. Behm, *Angew. Chem., Int. Ed.*, 2011, **50**, 10241–10245.
48 D. Widmann and R. J. Behm, *Acc. Chem. Res.*, 2014, **47**, 740–749.
49 I. X. Green, W. Tang, M. Neurock and J. T. Yates, *Science*, 2011, **333**, 736–739.
50 I. X. Green, W. Tang, M. Neurock and J. T. Yates, *Acc. Chem. Res.*, 2014, **47**, 805–815.
51 Y.-G. Wang, D. C. Cantu, M.-S. Lee, J. Li, V.-A. Glezakou and R. Rousseau, *J. Am. Chem. Soc.*, 2016, **138**, 10467–10476.
52 D. Widmann, A. Krautsieder, P. Walter, A. Brückner and R. J. Behm, *ACS Catal.*, 2016, **6**, 5005–5011.
53 Y. Denkwitz, Z. Zhao, U. Hörmann, U. Kaiser, V. Plzak and R. J. Behm, *J. Catal.*, 2007, **251**, 363–373.
54 P. Konova, A. Naydenov, C. Venkov, D. Mehandjiev, D. Andreeva and T. Tabakova, *J. Mol. Catal. A: Chem.*, 2004, **213**, 235–240.
55 C. K. Costello, M. C. Kung, H. S. Oh, Y. Wang and H. H. Kung, *Appl. Catal., A*, 2002, **232**, 159–168.
56 Z. Wu, D.-e. Jiang, A. K. P. Mann, D. R. Mullins, Z.-A. Qiao, L. F. Allard, C. Zeng, R. Jin and S. H. Overbury, *J. Am. Chem. Soc.*, 2014, **136**, 6111–6122.
57 L. D. Menard, F. Xu, R. G. Nuzzo and J. C. Yang, *J. Catal.*, 2006, **243**, 64–73.
58 S. Gaur, J. T. Miller, D. Stellwagen, A. Sanampudi, C. S. S. R. Kumar and J. J. Spivey, *Phys. Chem. Chem. Phys.*, 2012, **14**, 1627–1634.